IVYSPRING INTERNATIONAL PUBLISHER

International Journal of Biological Sciences

2027; 23(1): 391-406. doi: 10.7150/ijbs.136441

Research Paper

Eupalinolide B induces ferroptosis in activated HSCs to attenuate hepatic fibrosis via targeting peroxiredoxin 1

Yin-Kwan Wong[1#], Qian Zhang[2#], Min Zou[3#], Yu Chen[4#], Weiyi He[2], Yehai An[2], Dandan Liu[4], Ting Cao[2], Xiaoqin He[2], Juyi Tian[2], Qiwei Zhang[2], Yao Liang[2], Xuan Xiong[2], Xiaoyong Zhang[4✉], Wei Xiao[3✉], Jigang Wang[2,5,6✉], Ye Chen[1✉], Piao Luo[2✉]

1. Department of Gastroenterology, Shenzhen Hospital, Southern Medical University, Shenzhen 518101, China.
2. Guangdong Basic Research center of Excellence for Integrated Traditional and Western Medicine for Qingzhi Diseases, School of Traditional Chinese Medicine, Southern Medical University, Guangzhou 510515, China.
3. Guangdong Provincial Key Laboratory of New Drug Screening, School of Pharmaceutical Sciences, Southern Medical University, Guangzhou 510515, China.
4. Department of Gastroenterology, Nanfang Hospital, Southern Medical University, Guangzhou 510515, China.
5. State Key Laboratory for Quality Assurance and Sustainable Use of Dao-di Herbs, Artemisinin Research Center, and Institute of Chinese Materia Medica, China Academy of Chinese Medical Sciences, Beijing 100700, China.
6. Department of Pulmonary and Critical Care Medicine, Shenzhen Institute of Respiratory Diseases, Guangdong Provincial Clinical Research Center for Geriatrics, Shenzhen Clinical Research Center for Geriatrics, Shenzhen People's Hospital, The First Affiliated Hospital, School of Medicine, Southern University of Science and Technology, Shenzhen 518055, China.

# These authors made equal contributions to this work.

✉ Corresponding authors: Piao Luo (Email: luopiao@smu.edu.cn), Ye Chen (Email: yechen@smu.edu.cn), Jigang Wang (Email: jgwang@icmm.ac.cn), Wei Xiao (Email: xw7688@smu.edu.cn) and Xiaoyong Zhang (Email: xiaoyzhang@smu.edu.cn).

© The author(s). This is an open access article distributed under the terms of the Creative Commons Attribution License (https://creativecommons.org/licenses/by/4.0/). See https://ivyspring.com/terms for full terms and conditions.

Received: 2026.04.19; Accepted: 2026.09.07; Published: 2027.01.01

Abstract

Peroxiredoxin 1 (PRDX1), a pivotal member of the PRDX family, primarily scavenges hydrogen peroxide (H_2O_2). Effective inhibition of its expression or catalytic activity confers therapeutic effects in diseases including liver fibrosis and tumors. However, only a small subset of PRDX1 inhibitors has been reported so far, particularly covalent inhibitors targeting PRDX1. Herein, we report for the first time that Eupalinolide B (EuB) exerts anti-fibrotic effects by enhancing reactive oxygen species (ROS) production and triggering ferroptosis in activated hepatic stellate cells (HSCs). Chemical proteomics revealed that EuB covalently binds to PRDX1 *via* the α, β-unsaturated ketone moiety and inactivate its enzymatic activity. Furthermore, EuB promoted the accumulation of ROS and Fe^{2+}, reduced glutathione (GSH) levels, and downregulated glutathione peroxidase 4 (GPX4) expression. Additionally, site-directed mutagenesis confirmed that mutation of cysteine residues abrogated the binding of EuB to PRDX1, while LC-MS/MS analysis further verified the covalent binding of EuB to PRDX1 at Cys83. Notably, EuB-mediated ferroptosis and PRDX1 activity inhibition were effectively reversed by PRDX1 overexpression. Collectively, this study identifies EuB as a novel inhibitor of PRDX1, highlighting its great potential for the development of PRDX1-targeted anti-hepatic fibrosis agents.

Keywords: chemical proteomics; Eupalinolide B; hepatic fibrosis; peroxiredoxin 1; ferroptosis

1. Introduction

Hepatic fibrosis is a common intermediate stage in chronic liver diseases progression [1, 2], occurring particularly in individuals with congenital defects, viral infections [3], chemical metabolism disorders [4], or autoimmune diseases [5]. Once initiated, hepatic fibrosis can progressively advance to cirrhosis, which significantly elevates the risk of developing liver cancer [6]. Nevertheless, the molecular mechanisms underlying the pathogenesis of hepatic fibrosis are incompletely understood. Currently, there remains a lack of effective therapeutic agents to reverse or halt its progression.

Hepatic stellate cells (HSCs) play a pivotal role in the pathological progression of hepatic fibrosis [7]. Consequently, they have emerged as a key focus and critical target for investigating the pathological

mechanisms of hepatic fibrosis and developing therapeutic agents [8]. Previous studies have reported that the specific induction of apoptosis, autophagy, senescence, or ferroptosis in activated HSCs can inhibit the progression of hepatic fibrosis [9-13]. Recently, we have also demonstrated that the specific targeted inhibition of peroxiredoxins (PRDXs) induces redox homeostasis disruption, oxidative stress, and iron accumulation in activated HSCs [14], thereby triggering ferroptosis and ultimately suppressing the progression of hepatic fibrosis.

PRDXs represent a ubiquitously distributed family of antioxidant enzymes that additionally modulate cytokines, mediating signal transduction [15]. PRDXs utilize redox-active cysteine residues to reduce peroxide levels and are traditionally classified into two subgroups, 1-Cys and 2-Cys PRDXs, depending on the number of cysteinyl residues directly participating in catalysis [16, 17], with six isoforms (PRDX1-6) identified in mammals to date [18]. Among them, five 2-Cys PRDXs (PRDX1-5) use thioredoxin as their catalytic cycle electron donor, while PRDX6, the only 1-Cys PRDX, relies on glutathione (GSH) and GSH S-transferase (GST) to reduce its oxidized peroxidatic cysteine residue [19, 20]. Typical 2-Cys PRDXs such as PRDX1 are susceptible to overoxidation under high peroxide concentrations [21].

PRDX family members have been known to exert crucial regulatory functions in various liver diseases and hold promise as potential therapeutic targets. For instance, PRDX1 preserves mitochondrial function through scavenging H_2O_2, reducing lipid peroxidation, ultimately mitigating non-alcoholic steatohepatitis (NASH) progression [22]. PRDX1 knockdown in activated HSCs promotes lipid peroxidation (LPO) and iron ions accumulation, triggering ferroptosis to attenuate hepatic fibrosis progression [14]. Furthermore, hepatic PRDX1 overexpression improves liver function, alleviates hepatic oxidative stress, and regulates intracellular redox homeostasis in liver injury [23]. Therefore, the identification of novel inhibitors targeting PRDX1 provides new therapeutic strategies and drug candidates for chronic liver diseases, particularly hepatic fibrosis.

Traditional Chinese medicines (TCMs) possess distinctive advantages and great potential in the prevention and treatment of liver fibrosis [24, 25]. Numerous studies have confirmed that bioactive molecules isolated from medicinal plants exert significant anti-hepatic fibrosis effects by regulating core pathological processes such as oxidative stress, inflammatory responses, and hepatic stellate cell activation [14, 26, 27]. Notably, our previous studies have demonstrated that celastrol and glycyrrhetinic acid, two bioactive molecules derived from TCMs, target the PRDXs family in HSCs [14, 28], thereby effectively reversing the progression of liver fibrosis. EuB is a natural sesquiterpene lactone extracted from the medicinal plant *Eupatorium lindleyanum*. Our prior studies have demonstrated that it possesses potential anti-inflammatory and anti-tumor pharmacological activities [29, 30], whereas its therapeutic effects and underlying molecular mechanisms in liver fibrosis remain unelucidated.

This study aims to systematically investigate the interventional efficacy and underlying molecular mechanisms of EuB in combating liver fibrosis through both *in vitro* and *in vivo* experiments. We first assessed EuB's regulatory effects on key pathological hallmarks of the disease, including HSC activation and collagen deposition. Chemical proteomics approach was employed to identify the cellular targets of EuB, with a particular emphasis on verifying whether PRDX1 functions as its direct binding partner. We further demonstrated the molecular basis of the EuB-PRDX1 interaction, which is mediated by the α, β-unsaturated ketone moiety of EuB. Ultimately, we elucidated that EuB modulates the enzymatic activity of PRDX1 and its downstream signaling cascades, such as the expression of GPX4, iron ions accumulation, and ROS levels, thereby triggering ferroptosis in activated HSCs. Collectively, this study validates EuB as a potential PRDX1-targeted covalent inhibitor, laying a solid foundation for the development of novel therapeutic strategies against liver fibrosis.

2. Materials and Methods

Reagents

Cell Counting Kit-8 (CCK-8) was obtained from Solarbio Science & Technology Co., Ltd. (Beijing, China). EuB was acquired from Bethealth People Biomedical Technology Co., Ltd. (Beijing, China). N-acetyl-L-cysteine (NAC) and deferoxamine mesylate (DFO) were purchased from Abcam (Cambridge, UK). Reagents for click chemistry reactions were obtained from ClickChemistryTools (Scottsdale, AZ, USA) or Sigma-Aldrich (St. Louis, MO, USA). Reagents for liquid chromatography-tandem mass spectrometry (LC-MS/MS) were purchased from Thermo Fisher Scientific (Waltham, MA, USA) or Waters (Milford, MA, USA). The following primary antibodies were used: anti-PRDX1 (Abcam); anti-α-smooth muscle actin (α-SMA), anti-Vimentin (VIM), anti- fibroblast activation protein (FAP), anti- collagen type I alpha 1 (COL1A1), anti-heme oxygenase 1 (HO-1), anti-GPX4, anti-β-actin, and anti-glyceraldehyde-3-phosphate

dehydrogenase (GAPDH) (Proteintech Group, Inc., Wuhan, China).

Cell viability assay

Human hepatic stellate cells (LX-2) were cultured and seeded into 96-well plates, and incubated with EuB or Eupalinolide B-probe (EuB-p). When the cell confluency reached 70-80%, its viability was determined using the CCK-8 kit.

Animal experiments

All animal experiments were approved by the Animal Care and Use Committee of Southern Medical University (Guangzhou, China), and all procedures were performed in accordance with the Guide for the Care and Use of Laboratory Animals. Male C57BL/6 mice (7 - 8weeks, 22 ± 2 g) were randomly divided into 5 groups (n = 8 per group): control group (vehicle), carbon tetrachloride (CCl_4)-induced model group, CCl_4 + EuB (2.5 or 5 mg/kg) group and CCl_4 + Silymarin (100 mg/kg) group. For the CCl_4-induced hepatic fibrosis model [14, 31], the control group received vehicle (olive oil) via intraperitoneal injection. EuB was dissolved in a vehicle composed of 5% dimethyl sulfoxide (DMSO), 30% polyethylene glycol 300, and 65% normal saline, and administered to the subjects via intraperitoneal injection for a consecutive period of 4 weeks. Silymarin was selected as the positive control in this study [32]. At the end of the experiment, all mice were anesthetized with isoflurane, followed by collection of serum and liver tissue samples for subsequent analyses.

Biochemical and histological assays

Serum was collected from anesthetized mice and stored. Serum biochemical parameters were analyzed as described previously [33]. Liver tissues were fixed, embedded, and sectioned into slices. Samples were stained by hematoxylin and eosin (H&E) kit for histological evaluation of liver injury, and Masson's trichrome as well as Sirius Red staining for collagen deposition measurement.

Immunohistochemical assay

For immunohistochemical staining, primary antibodies (COL1A1 and α-SMA) were used, followed by visualization with the HRP-DAB Cell & Tissue Staining Kit (ZSGB-BIO, Beijing, China).

Immunofluorescent staining

LX-2 cells were seeded in glass-bottom dishes. Cells were then incubated with EuB-P or DMSO (vehicle control). After incubation, cells were fixed and permeabilized. Samples were then incubated with a pre-prepared click reaction cocktail with gentle shaking at RT. After the click reaction, cells were washed to remove unreacted reagents. For immunofluorescence co-localization analysis, cells prepared as described above were blocked and incubated with primary antibodies. Cells were then incubated with secondary antibodies (Abcam). Subsequently, nuclei were stained with Hoechst 33342. Finally, all images were obtained using a confocal laser scanning microscope.

Determination of Lipid Peroxidation, iron ions Level, and Antioxidant Capacity

The following kits and probes were purchased for related detections: malondialdehyde (MDA) assay kit, GSH assay kit, fluorescent probe (CM-H_2DCFDA), total superoxide dismutase (SOD) assay kit, and hydrogen peroxide (H_2O_2) assay kit, all from Beyotime Biotechnology Co., Ltd. (Shanghai, China). Additionally, ferrous iron colorimetric assay kit and cell ferrous iron colorimetric assay kit were obtained from Elabscience Biotechnology Co., Ltd. (Wuhan, China).

Western blot

Cell or tissue proteins were extracted, followed by electrophoresis. Samples were treated with primary and secondary antibodies. Protein bands were visualized using enzyme-linked chemiluminescence and analyzed by ImageJ software.

Quantitative real-time PCR (qPCR)

Total RNA was extracted from samples. qPCR was performed using qRT-PCR Kit. GAPDH served as the internal control for qPCR. All primers used for qPCR are listed in Table S1.

Fluorescence labeling assay

For the fluorescence labeling assay, the experimental procedure was performed as described previously [14]. Briefly, cells were seeded in culture plates and treated with or without EuB-P. Total proteins were extracted from the cells, and soluble proteins from different groups were incubated with the click chemistry reaction cocktail. Labeled proteins were subsequently precipitated with pre-chilled acetone, resuspended in loading buffer, and separated by SDS-PAGE. Fluorescence signals were visualized via fluorescence scanning using a laser scanner, followed by Coomassie brilliant blue (CBB) staining. For the fluorescence labeling of proteins, the proteins were pre-treated with or without competitors prior to incubation with the probe. After probe incubation, samples were subjected to the pre-mixed click chemistry cocktail for conjugation. The samples were then separated by SDS-PAGE and visualized using the

same fluorescence scanning protocol as described above.

Target identification

EuB-P was first used to treat LX-2 for 1h. The probe or DMSO was then replaced and cells were rested for 3h. We extracted the soluble proteins and added the click reaction cocktail, shaking at 21 °C for 2h. After acetone precipitation of the labeled proteins, we used SDS to dissolve the samples, and then diluted it. At the same time, we washed the streptavidin beads (Thermo) and added them to the samples for overnight incubation at 4 °C. For pull down-TMT, the samples were washed successively with 6M urea and various concentrations of SDS and the samples were reduced and alkylated. Samples were incubated with trypsin for digestion and then desalted. Finally, peptides were labeled with TMT10 plex Mass Tag and then analyzed by LC-MS/MS (Thermo). For pull down-Western blot analysis, the binding protein was accessed by Western blot assay following the identical protocols outlined previously [33].

CETSA-Western Blot (CETSA-WB) Assay

Total cellular protein was extracted as described previously [34-36]. Protein samples from the DMSO group and EuB treatment group were prepared. Each protein sample was divided into 10 aliquots, which were subjected to gradient heating (37–73 °C) using a thermocycler (Applied Biosystems, Thermo Fisher Scientific, Waltham, USA) with programmed temperature increments. After heating, samples were centrifuged to pellet insoluble protein aggregates. The resulting supernatants were collected for subsequent Western blot analysis as described above.

Recombinant protein purification

The full-length human PRDX1 gene and its mutant constructs were subcloned into pET-28a vectors (Sangon Biotech Co., Ltd., Shanghai, China). The Escherichia coli BL21 was transformed and cultured in LB medium. Protein expression was induced with IPTG. The bacterial pellets were suspended in lysis buffer and disrupted by sonication. The supernatant obtained by centrifugation was applied to Ni-NTA beads column and then acquired recombinant protein.

Peroxidase activity assay

The peroxidase activities of PRDXs were detected as described previously [37], followed by using H_2O_2 kit (Beyotime). PRDX1 protein and lysate incubated with DMSO or EuB, followed by measurement as described above.

Plasmids with overexpressing PRDX1 assay

LX-2 cells were transfected with negative control (NC) vector and PRDX1-overexpressing plasmid by using Lipofectamine™ 3000 Transfection Reagent (Thermo) strictly following the manufacturer's instructions.

Proteomics analysis

LX-2 cells or mouse liver tissues were collected and lysed in buffer. Protein concentration of each sample was determined. For protein reduction, DTT was added to the samples; IAA was added to achieve alkylation. Subsequently, trypsin was added to the samples, and digestion was performed overnight at 37 °C. Peptides were desalted using a commercial C18 column and then analyzed by LC-MS/MS. Differentially expressed proteins (DEPs) among the control (DMSO), model, and EuB treatment groups were identified based on protein abundance intensity. DEPs were filtered using the criteria of absolute fold change (FC) ≥ 1.5 and adjusted p-value < 0.05. Volcano plots were generated to visualize DEPs using the "ggplot2" package in R software. Furthermore, Gene Ontology enrichment analysis was performed on the filtered DEPs using the "clusterProfiler" R package with default parameters.

Molecular docking and dynamics simulation

The PRDX1 structure was retrieved from the AlphaFold Protein Structure Database. Prior to molecular docking, PRDX1 protein structures were processed by PyMOL 2.5.2 to dismiss water molecules and add hydrogen atoms. Molecular docking simulation between PRDX1 and EuB was performed by AutoDock Vina, with the grid box centered on the active site of PRDX1, and was visualized and analyzed using PyMOL 2.5.2.

For molecular dynamics (MD) simulations, the optimal docking conformations generated by AutoDock Vina were used as initial structures. The MD system was first subjected to energy minimization and pressure equilibration using GROMACS 2025.1. Subsequently, a 100 ns MD simulation was conducted under the NPT ensemble. Post-simulation analysis was performed using gmx_MMPBSA to calculate the conventional energy decomposition terms.

Statistical analysis

All data are presented as the mean ± standard deviation (SD) from at least three independent experiments. Statistical analyses were performed using GraphPad Prism 9.0 software (GraphPad Software, USA). For multiple comparisons, one-way analysis of variance (ANOVA) was applied followed

by Tukey's test. For comparisons between two groups, an unpaired two-tailed Student's t-test was used.

3. Results

EuB alleviates CCl_4-induced hepatic fibrosis in mice

To assess the pharmacological effects of EuB on CCl_4-induced liver fibrosis in mice, we first established the animal experimental protocol as illustrated in Figure 1A-B. Histopathological analysis showed that EuB and Silymarin significantly ameliorated CCl_4-induced liver injury, restored the hepatic lobular architecture, and reduced inflammatory cell infiltration (Figure 1C). EuB and Silymarin treatment decreased the liver weight-to-body weight ratio, mitigated CCl_4-induced hepatomegaly, and significantly reduced the aspartate transaminase (AST) and alanine transaminase (ALT) levels, collectively indicating improved liver function (Figure 1D-F). Furthermore, Masson and Sirius Red staining demonstrated that EuB and Silymarin markedly reduced collagen deposition in liver tissues (Figure 1G-I). This finding was further validated by immunohistochemical staining for α-SMA (a marker for activated-HSCs) and COL1A1 in a dose-dependent manner (Figure 1G and Figure 1J-K), which further validated the selection of 5 mg/kg EuB for subsequent mechanistic investigations. EuB inhibited the protein expression of α-SMA, VIM, and COL1A1 (Figure S1A-D). Meanwhile, qPCR assays showed that EuB downregulated the mRNA expression of COL1A1, α-SMA, collagen type III alpha 1 (COL3A1), tissue inhibitor of metalloproteinase 1 (TIMP1), FAP and transforming growth factor-β (TGF-β), thereby attenuating liver fibrosis *in vivo* (Figure S1E). Taken together, these findings confirm that EuB effectively alleviates CCl_4-induced liver injury and hepatic fibrosis in mice.

EuB ameliorates liver fibrosis by regulating ROS and ferroptosis signaling pathways

To further elucidate how EuB ameliorates hepatic fibrosis *in vivo*, we carried out proteomics to explore the intervention mechanism of EuB in the Model group (Figure 2A). Our data shows a large number of differential expression proteins (DEPs) between the Model and Control groups (red up 586 and blue down 455 proteins) (Figure 2B and Figure S2A). DEPs were filtered using the criteria of absolute fold change (FC) ≥ 1.5 and adjusted *p*-value < 0.05. After EuB treatment, the DEPs in the Model group were significantly reversed (blue down 506 and red up 301 proteins) (Figure 2C and Figure S2B). As depicted in the Venn Diagram, there are 1041 DEPs between Control and Model, 807 DEPs between EuB and Model, and 345 overlapping DEPs between the two comparisons, suggesting that these proteins may be the core targets of EuB intervention (Figure 2D). The expression pattern clustering of DEPs among the three groups intuitively reflects the consistency of protein expression differences and grouping among the Control, Model, and EuB groups (Figure 2E). The DEPs are mainly participating in biological processes, including apoptotic process, inflammatory response, cytoskeletal organization, and response to oxidative stress, suggesting that these pathways may play key roles in model pathology and EuB intervention (Figure 2F). We found that EuB significantly downregulated the expressions of hepatic fibrosis-related proteins (α-SMA, COL1A1, COL3A1, TGF-β, VIM, etc.) in the Model group (Figure 2G-K and Figure S2C-G), indicating that EuB could inhibit hepatic fibrosis progression. Moreover, the expressions of ferroptosis- and oxidative stress-related proteins (KEAP1, HO-1, GPX4, etc.) were elevated in the Model group, and reversed after EuB treatment (Figure 2L-P and Figure S2H-I). These results indicate that EuB mitigates liver fibrosis by regulating ROS and ferroptosis signaling pathways in mice. Notably, these bulk-liver proteomic signals reflect aggregated protein abundance across heterogeneous liver cell populations (hepatocytes, macrophages, activated HSCs and other non-parenchymal cells), rather than changes restricted solely to activated HSCs. We therefore performed subsequent *in vitro* assays using activated HSCs to investigate whether EuB treatment modulates the expression of proteins including GPX4 and HO-1 within activated HSCs and thereby triggers ferroptosis.

EuB suppresses pro-fibrotic factor expression *via* inducing ferroptosis in activated HSCs

For a deeper understanding of the molecular mechanisms underlying EuB-mediated anti-hepatic fibrosis activity, we performed pharmacological mechanism studies on activated HSCs. Initially, we observed that EuB significantly inhibited the transcriptional levels of pro-fibrotic genes, including α-SMA, COL3A1, TIMP1 and COL1A1 (Figure 3A and Figure S3A). We carried out proteomics to explore the intervention mechanism of EuB in activated HSCs. Results showed a large number of differential proteins between activated HSCs (DMSO) and the EuB group, EuB significantly inhibited the expressions of extracellular matrix, inflammatory response, oxidative stress and ferroptosis proteins in activated HSCs (Figure 3B-C and Figure S3B-C). Venn Diagram showed that there are 556 DEPs between EuB-6 and DMSO, 1656 differential proteins between EuB-12 and

DMSO, and 426 overlapping DEPs between the two comparisons, suggesting that these proteins could be key targets of EuB intervention (Figure 3D). We have also depicted these DEPs among the three groups as a Heatmap (Figure 3E). The DEPs are involved in biological processes, including extracellular matrix, inflammatory response, oxidative stress and ferroptosis (Figure 3F). We found the expressions of activated HSCs-related proteins (COL1A1, COL5A1, COL6A1, TGF-βR1, etc.) to be significantly downregulated after EuB treatment (Figure 3G and Figure S3E-F), indicating that EuB could inhibit HSCs activation. Moreover, the expression pattern of ferroptosis- and oxidative stress-related proteins (KEAP1, HO-1, GPX4, etc.) was partially reversed after EuB treatment (Figure 3H-I and Figure S3G-H). These results indicate that EuB suppresses pro-fibrotic factor expression through regulating ROS and ferroptosis signaling in activated HSCs.

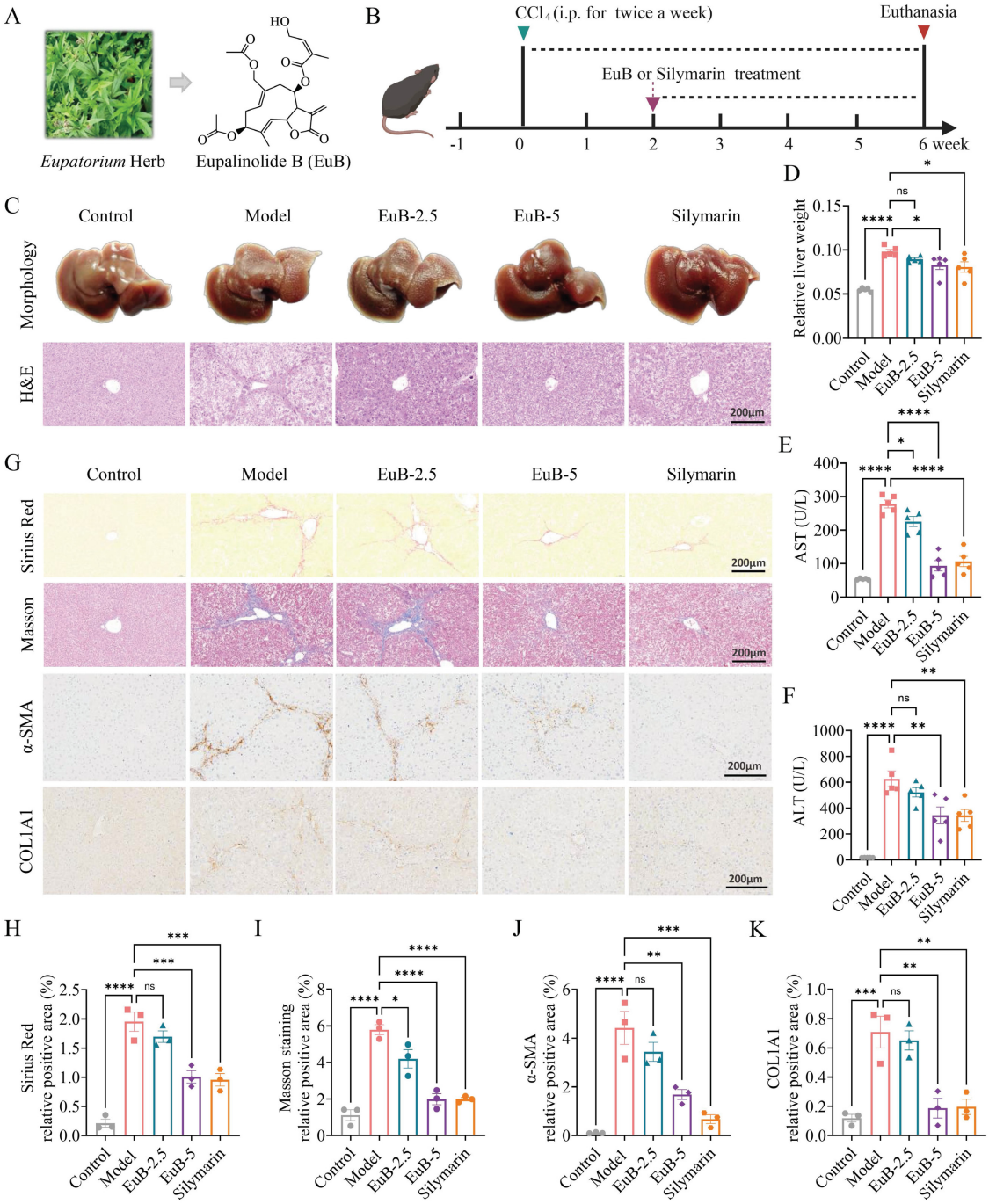


Figure 1. EuB mitigates liver injury and fibrosis in mice. (A) the *Eupatorium* herb and the structure of EuB. (B) Experimental scheme of animal experiments, EuB (2.5 mg/kg or 5 mg/kg). (C) Representative photographs of mouse livers, H&E staining (scale bar = 200 μm). (D-F) Liver weight-to-body weight ratio, AST and ALT in mice (n = 5-8). (G) Immunohistochemistry staining of a-SMA and COL1A1 (Scale bar = 200 μm). (H-I) Statistical analysis of Masson and Sirius Red staining (n = 3). (J-K) Statistical analysis of immunohistochemistry staining for α-SMA and COL1A1 (n = 3). Mean ± SD, *$p < 0.05$, **$p < 0.01$, ***$p < 0.001$, ****$p < 0.0001$ *vs.* Model.

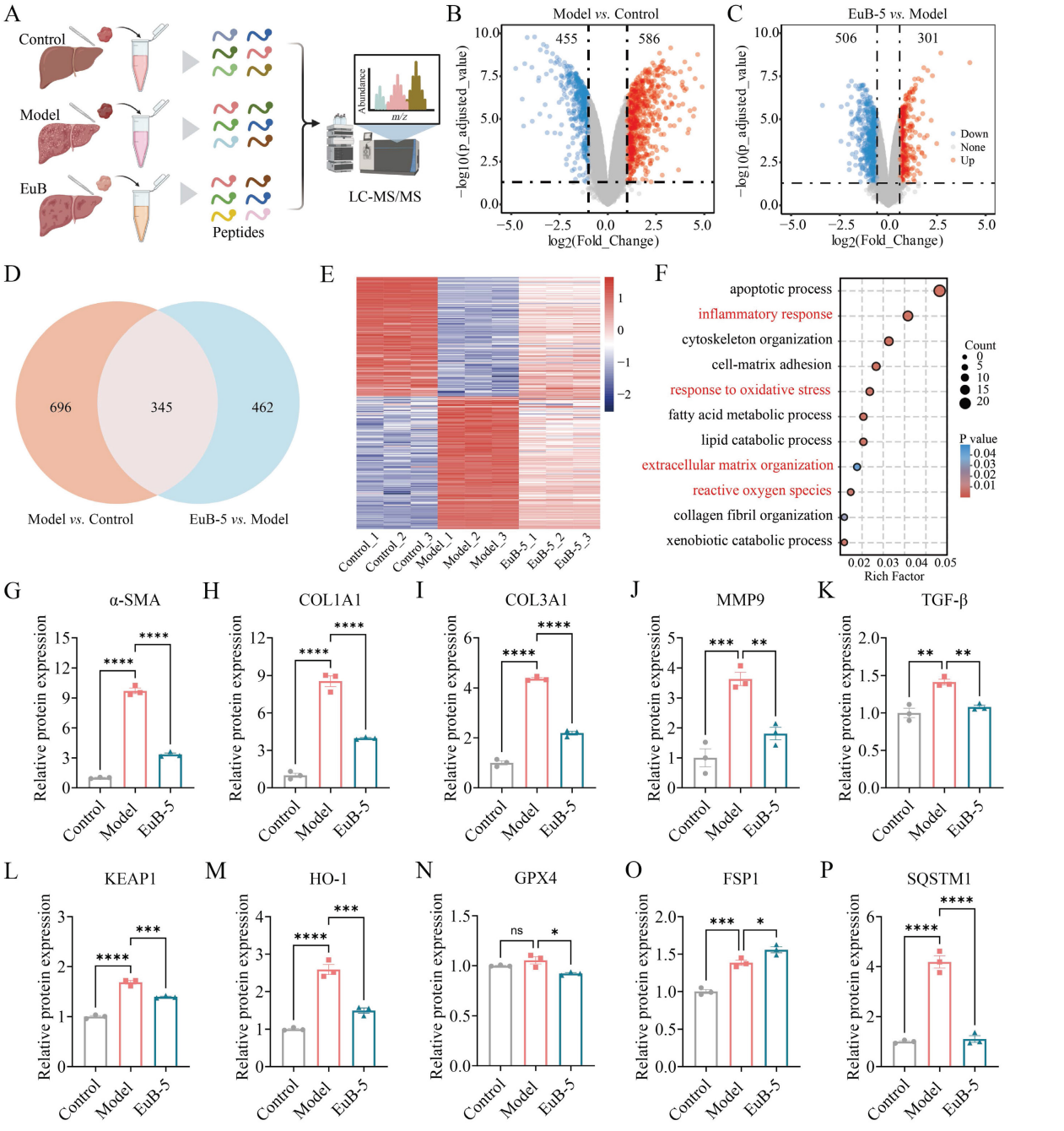


Figure 2. Proteomic analysis reveals that EuB ameliorates liver injury in mice by regulating ROS-mediated fibrosis and ferroptosis pathways. (A) Experimental scheme of proteomic analysis, EuB (5 mg/kg). (B-C) Volcano plots to visualize DEPs profiles. (D) Venn diagram illustrating the overlap of DEPs. (E) Heatmap of hierarchical clustering analysis for the overlapping DEPs. (F) Functional enrichment analysis of the DEPs. (G-K) Protein expression levels of hepatic fibrosis-related markers by proteomic analysis (n = 3). (L-P) Protein expression levels of ferroptosis- and oxidative stress-related molecules (n = 3). Mean ± SD, *$p < 0.05$, **$p < 0.01$, ***$p < 0.001$, ****$p < 0.0001$ *vs.* Model group. KEAP1, Kelch-like ECH-associated protein 1; FSP1, Ferroptosis suppressor protein 1; SQSTM1, Sequestosome 1.

Concomitantly, Western blotting demonstrated that EuB downregulated the protein expression of FAP, VIM, and α-SMA in activated HSCs (Figure 3J and Figure S3D). In our previous work, we demonstrated that natural products can exert anti-hepatic fibrosis effects by directly inducing ferroptosis in activated HSCs [14]. Our data also demonstrated that EuB exerts its anti-fibrotic activity through ROS and ferroptosis signaling. EuB downregulated the expression of GPX4 (a key negative regulator of ferroptosis) in activated HSCs while upregulating the expression of HO-1 (Figure 3K). Additionally, qPCR assay confirmed that EuB inhibits GPX4 expression and upregulates the expressions of Nrf1 and HO-1 (Figure S3I). Notably, HO-1 catalyzes the free heme degradation into Fe^{2+}, biliverdin, and carbon monoxide [38], a process closely linked to ferroptosis and oxidative stress. Further investigations revealed that EuB triggered iron accumulation in activated HSCs (Figure 3L). EuB effectively induced ROS

accumulation in activated HSCs, while this effect was markedly attenuated by the ROS scavenger NAC (Figure 3M). Additionally, EuB reduced the antioxidant enzyme SOD activity and the intracellular level of the ferroptosis inhibitor GSH, and NAC treatment partially reversed these reductions (Figure 3N-O). Collectively, these results indicate that EuB suppresses pro-fibrotic factor expression *via* inducing ferroptosis in activated HSCs.

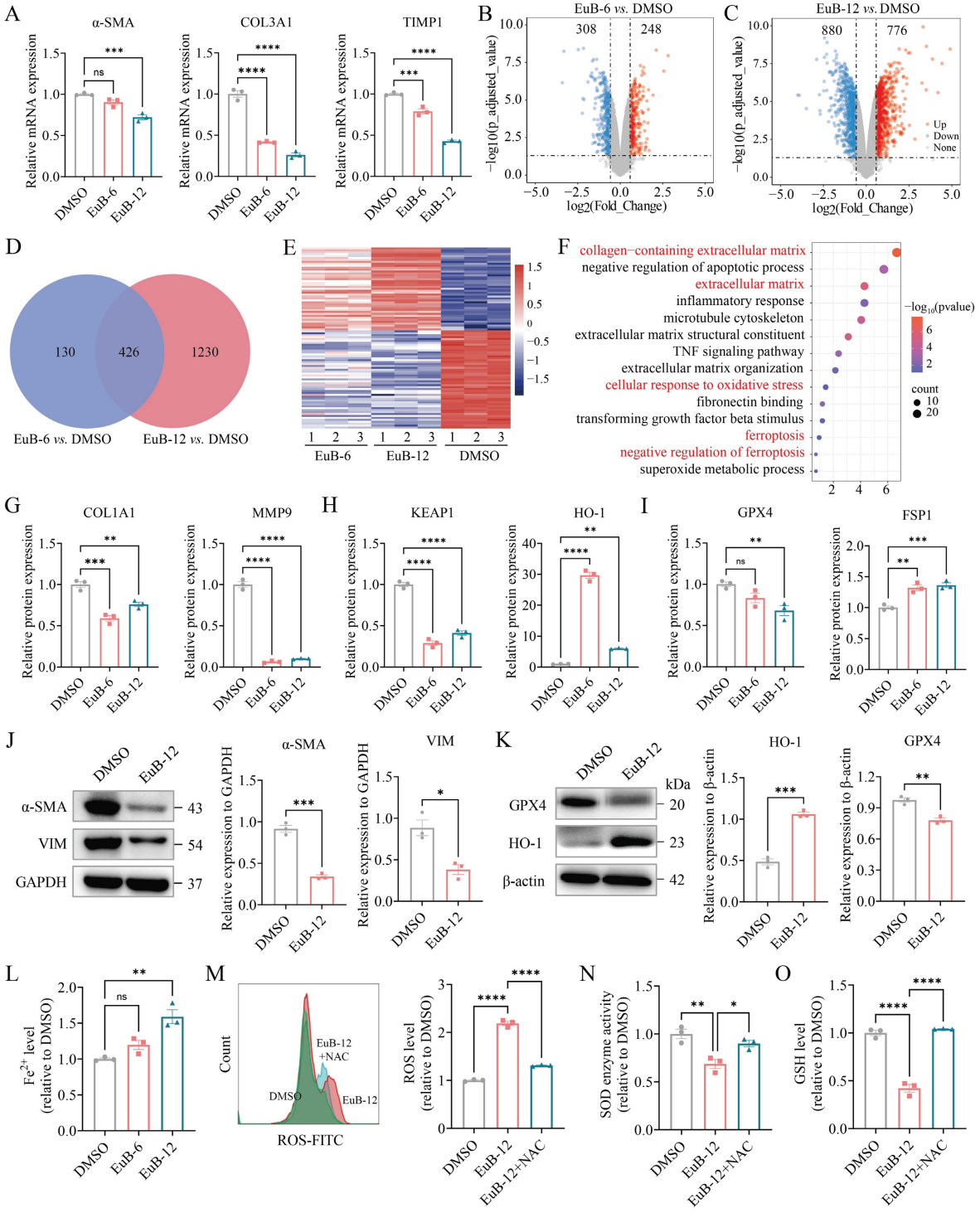


Figure 3. EuB suppresses pro-fibrotic factor expression via activating ROS signaling and inducing ferroptosis in activated HSCs. (A) The mRNA expressions of fibrosis-associated markers, EuB (6 or 12 μM) (n = 3). (B-C) Volcano plots to visualize the DEPs in activated HSCs. (D) Venn diagram illustrating the overlap of DEPs. (E) Heatmap of hierarchical clustering analysis for the overlapping DEPs. (F) Functional enrichment analysis. (G) Protein expression levels of hepatic fibrosis-related markers by proteomic analysis (n = 3). (H-I) Protein expression levels of ferroptosis- and oxidative stress-related molecules (n = 3). (J) Western blot of the VIM and a-SMA protein expressions (n = 3). (K) Western blot of GPX4 and HO-1 protein expressions (n = 3). (L) Detection of the iron ions level in activated HSCs treated with EuB (n = 3). (M) Detection of ROS generation by flow cytometric analysis in activated HSCs treated (n = 3). (N-O) The antioxidant enzyme SOD activity and GSH level in activated HSCs treated with EuB and EuB+NAC (n = 3). Mean ± SD, *p < 0.05, **p < 0.01, ***p < 0.001, ****p < 0.0001 *vs.* DMSO or EuB-12.

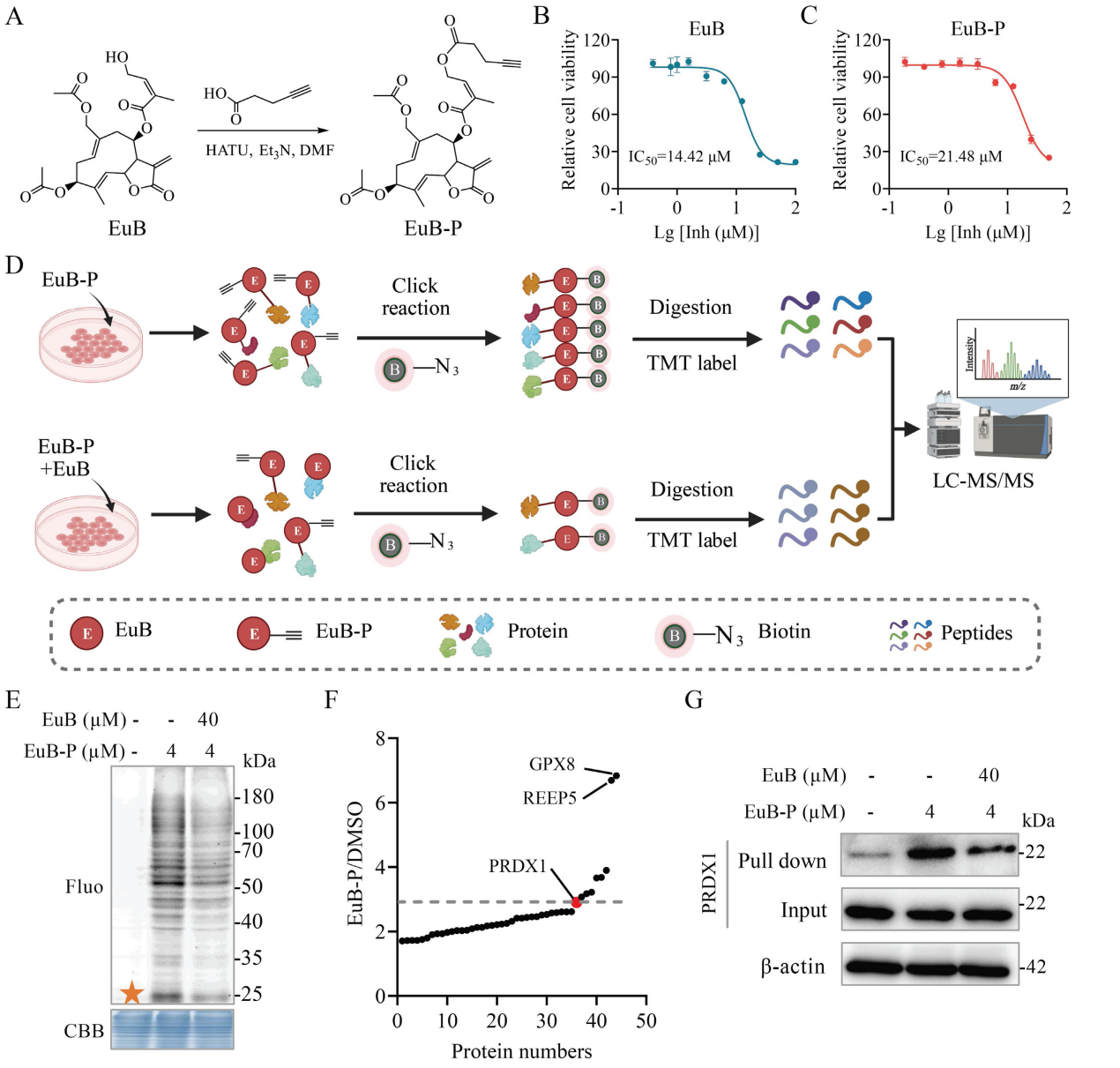


Figure 4. EuB directly binds to PRDX1 identified by chemical proteomics. (A) Structures of EuB and EuB-P. (B-C) CCK-8 assay for viability of LX2 cells treated with EuB or EuB-P. (D) Workflow of the chemical proteomics approach. (E) EuB-P labeling of potential target proteins in LX2 cells with or without excess EuB. (F) Quantification of TMT EuB-P/DMSO group ratio in LX2 cells via competitive experiment. (G) Pull-down assay verifying the interaction between EuB and PRDX1.

Chemical proteomics identifies PRDX1 as a direct binding target of EuB

To explore the mechanism by which EuB activates ROS signaling and induces ferroptosis in activated HSCs, we aimed to identify potential EuB-binding proteins. For this purpose, an alkyne-tagged EuB probe (EuB-P) was chemically synthesized (Figure 4A). CCK8 assay results showed that EuB effectively inhibited the proliferation of activated HSCs (LX2). Importantly, EuB-P exerted a comparable inhibitory effect on activated HSCs to EuB (Figure 4B-C), indicating that the introduction of the alkyne tag had minimal impact on the biological effect of EuB. Subsequently, potential target proteins of EuB were identified by chemical proteomics in activated HSCs (Figure 4D). First, cells were labeled with the EuB-P; thereafter, EuB-P-bound proteins were visualized by conjugating a fluorescent tag through click chemistry (Figure S4A and Figure S4B). Additionally, a competition assay was conducted to assess whether EuB could compete with EuB-P-bound target proteins. The results revealed that a specific band corresponding to EuB-P-bound proteins at approximately 25 kDa was significantly reduced upon treatment with excess EuB (Figure 4E).

This specific protein band was further analyzed using TMT labeling combined with LC-MS/MS quantification. In the high-confidence proteins subjected to credibility comparison, GPX8 and PRDX1

are mainly closely related to biological processes including oxidative stress and ferroptosis. Even though GPX8 had a higher TMT ratio (Figure 4F and Figure S4C), PRDX1's advantages in peptide count, peptide-spectrum matches (PSMs) count, and identification confidence made it a more robust candidate (Figure S4C). This choice was made to increase the success rate and credibility of follow-up validation experiments. Notably, PRDX1 has been reported as an important antioxidant regulator and a potential regulator of ferroptosis [14]. We verified the direct interaction between EuB and PRDX1 protein with a pull-down assay, and PRDX1 was also successfully pulled down by EuB-P (Figure 4G). In summary, these findings indicate that EuB directly binds to PRDX1.

EuB directly binds to the cysteine residues of PRDX1

To further validate the interaction between EuB and PRDX1, we performed CETSA-WB assay. Results showed that EuB significantly enhanced the thermal stability of PRDX1 (Figure 5A and Figure 5B). Concurrently, immunofluorescence co-localization assays were performed using EuB-P and PRDX1. The results showed a distinct co-localization pattern of EuB-P and PRDX1 (Figure 5C). Moreover, recombinant human PRDX1 (rhPRDX1) and rhPRDX2 were treated with EuB-P *via* click chemistry. As expected, EuB-P specifically and efficiently bound to rhPRDX1, whereas no obvious fluorescent signal was detected in the rhPRDX2 group (Figure 5D and Figure S5A), and this labeling was competitively abrogated by excess unmodified EuB, IAA (Iodoacetamide, a well-characterized cysteine alkylating reagent), or celastrol (Cel) (Figure 5E). Notably, it has previously been confirmed that Cel binds specifically to the cysteine residues of PRDXs [37]. To further confirm EuB binding to PRDX1 cysteines, we labeled rhPRDX1 with the IAA-derived probe (IAA-P), followed by conjugation to fluorescent tags via click chemistry. Excess EuB, Cel, or IAA effectively competed with IAA-P for rhPRDX1 binding (Figure 5F-G), further confirming EuB's direct binding to PRDX1's cysteine residues.

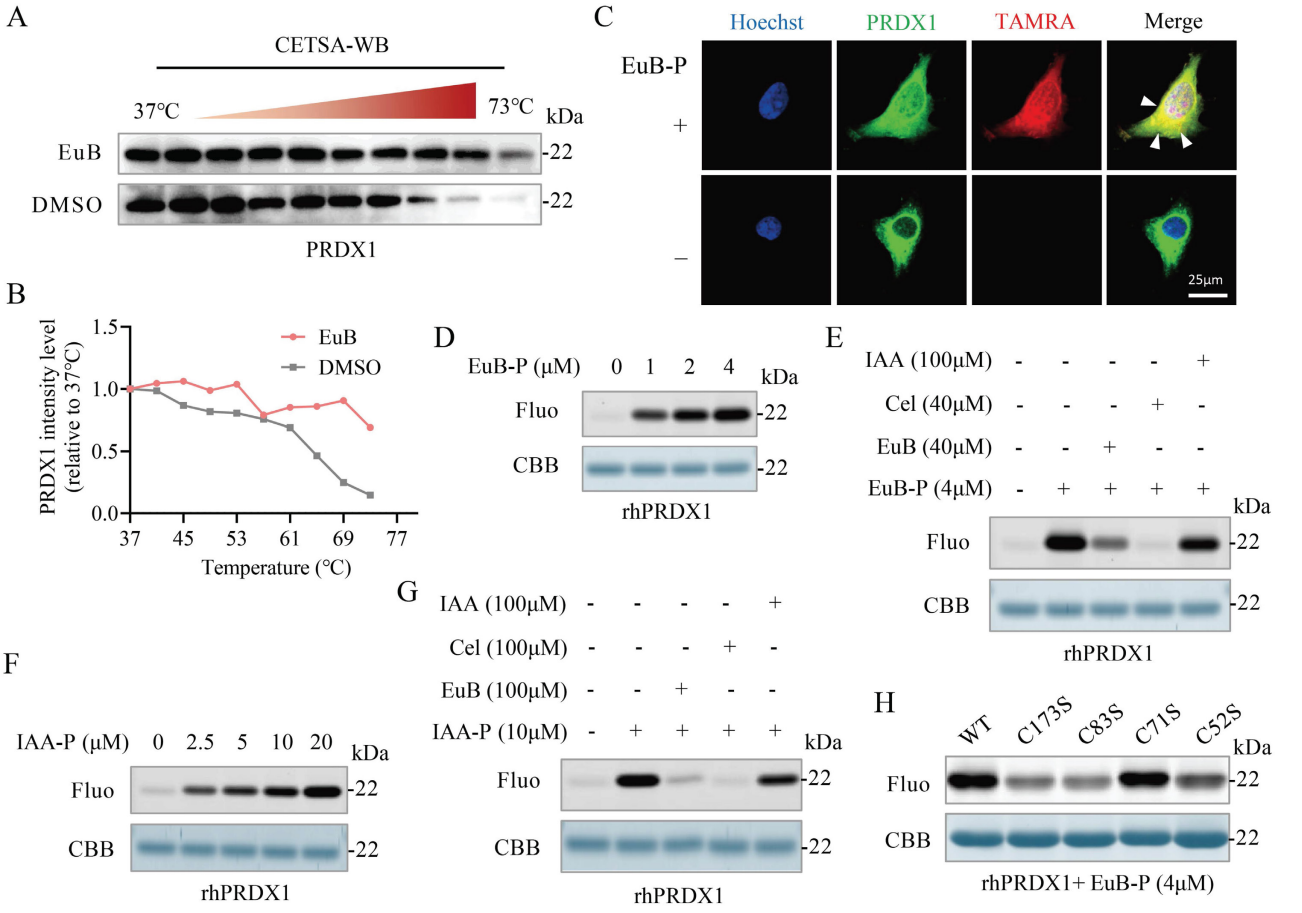


Figure 5. EuB directly binds to the cysteine residues of PRDX1. (A-B) CETSA-WB assay. (C) Immunofluorescence of PRDX1 (green) and EuB-P (red) in LX2 cells. Scale bar = 25 μm. (D) The labelling of rhPRDX1 by EuB-P. (E) EuB-P labelling rhPRDX1 protein with or without excess EuB, Cel or IAA. (F) The labeling of rhPRDX1 by the IAA-P. (G) IAA-P labelling rhPRDX1 protein with or without excess EuB, Cel or IAA. (H) Mutation analysis on cysteine sites of WT or mutants recombinant PRDX1.

Subsequently, site-directed mutagenesis was performed on the cysteine residues of PRDX1 to construct a panel of cysteine-mutated variants. The rhPRDX1 mutants were first labeled with EuB-P, then subjected to a click reaction with an azide dye. The results indicated that the fluorescence intensity of the PRDX1 Cys83 mutant labeled by EuB-P exhibited the most significant reduction among the four mutants (Figure 5H). To map the EuB-binding site on PRDX1, we performed molecular docking analysis between EuB and PRDX1 structure. The docking results revealed a direct interaction between EuB and Cys83 of PRDX1 (Figure S5B). Collectively, our findings reveal that EuB directly binds to Cys83 of PRDX1 (Figure S5C).

EuB covalently binds to the Cys83 of PRDX1 *via* its α, β-unsaturated ketone moiety

Given that the α, β-unsaturated ketone moiety of EuB is highly likely to function as a reactive Michael acceptor capable of forming covalent bonds with Cys residue(s) in proteins, we sought to further confirm the specific Cys residue(s) modified by EuB. To this end, rhPRDX1 protein was incubated in the presence or absence of EuB, followed by LC-MS/MS analysis. EuB exhibits an exact molecular weight of 462.19 at m/z, and a database search for protein MS/MS spectra was performed using a mass increment of 462.19 Da. Our data also confirmed that the Cys83-containing peptide (LNCQVIGASVDSHFCHLAWVNTPK) showed a 462.19 Da mass shift in the EuB-treated group (Figure 6A-B), as evidenced by the y13 to y18 fragment ions. The mass shift detected is in agreement with the addition of one EuB residue molecular unit (462.19 Da) (Figure 6C). However, this mass shift was not observed in other Cys-containing peptides. Collectively, these data directly confirm that EuB covalently binds to PRDX1 in a site-selective manner, with this interaction preferentially and site-selectively occurring at the Cys83 residue rather than at other cysteine sites.

Next, we performed MD simulations of the Cys83 residue in PRDX1 with EuB. A 100 ns MD simulation confirmed the stability of the EuB-PRDX1 complex through changes in root-mean-square deviation (RMSD), radius of gyration (Rg), solvent accessible surface area (SASA), and root-mean-square fluctuation (RMSF) (Figure S6A-D). The Lennard-Jones (LJ)-SR plot shows the potential energy change curve around the Cys83 residue, reflecting the spatial interactions before and after EuB binding (Figure 6D). Dynamic changes in the number of hydrogen bonds formed at the Cys83 residue indicate a direct interaction between EuB and the Cys83 residue (Figure 6E). Additionally, the change in the coulomb (Coul)-SR of Cys83 reflects the effect of EuB modification on the exposure of this residue (Figure 6F). The conformational energy landscape of the EuB-treated group shows a significant alteration in conformational distribution (Figure 6G), demonstrating that EuB binding to the Cys83 residue of PRDX1 impairs the overall conformational stability of PRDX1. In summary, these results provide further robust evidence that EuB preferentially and site-selectively binds to the Cys83 residue of PRDX1.

EuB inhibits PRDX1 enzymatic activity to induce ferroptosis in activated HSCs and exerts an ameliorative effect on hepatic fibrosis

We next assessed PRDX1 protein expression in LX-2 cells and CCl_4-induced mouse models following EuB treatment. Results revealed that EuB exerted negligible effects on PRDX1 expression (Figure 7A and Figure S7A). We further investigated whether EuB impairs the antioxidant activity of cellular lysates or rhPRDX1 using a H_2O_2 reduction assay. As shown, EuB significantly suppressed both the peroxidase activity of rhPRDX1 and the cellular PRDX enzymatic activity responsible for H_2O_2 scavenging (Figure 7B-C). Concomitantly, EuB induced a concentration-dependent (3, 6, and 12 μM) increase in intracellular ROS, indicative of EuB-mediated ROS accumulation (Figure S7B). In parallel, EuB promoted iron ions accumulation; notably, this effect was largely abrogated by the iron chelator DFO (Figure 7D), suggesting that EuB may participate in iron metabolism regulation or ferroptosis induction. To define PRDX1's functional role, we established a PRDX1 overexpression system (Figure 7E). Western blotting analysis of α-SMA demonstrated that EuB treatment reduced α-SMA expression in PRDX1 overexpression HSCs (Figure S7C-D). Additionally, PRDX1 overexpression attenuated EuB's inhibitory impact on PRDX enzymatic activity (Figure 7F), while also mitigating EuB-induced elevation of MDA (a lipid peroxidation marker), iron ions accumulation (Figure 7G and Figure S7E) and reduction of GSH (an antioxidant) and GPX4 expression (Figure 7H and Figure S7F) levels. Collectively, these findings confirm that EuB suppresses PRDX1 enzymatic activity without affecting its expression, which in turn results in ROS generation and triggers ferroptosis, ultimately contributing to the amelioration of hepatic fibrosis by EuB (Figure 8).

4. Discussion

As a canonical 2-Cys antioxidant enzyme, PRDX1 is predominantly localized in the cytosol, where it critically maintains cellular redox homeostasis

through scavenging intracellular peroxide, thereby exerting potent anti-oxidative stress effects [22]. Accumulating evidence has shown that PRDX1 inhibition or deficiency elevates intracellular ROS and induces cellular damage [39-41]. Moreover, it has been demonstrated that PRDX1 exerts a critical effect on the pathogenesis of liver diseases [14, 22, 42]. Therefore, selective PRDX1 inhibition represents a potential therapeutic approach for hepatic diseases, such as hepatic fibrosis, by specifically disrupting redox homeostasis in pathogenic cells, including activated HSCs in hepatic fibrosis [14]. However, few PRDX1 inhibitors have been discovered, which has hindered the advancement of PRDX1- targeted therapies for liver-related diseases.

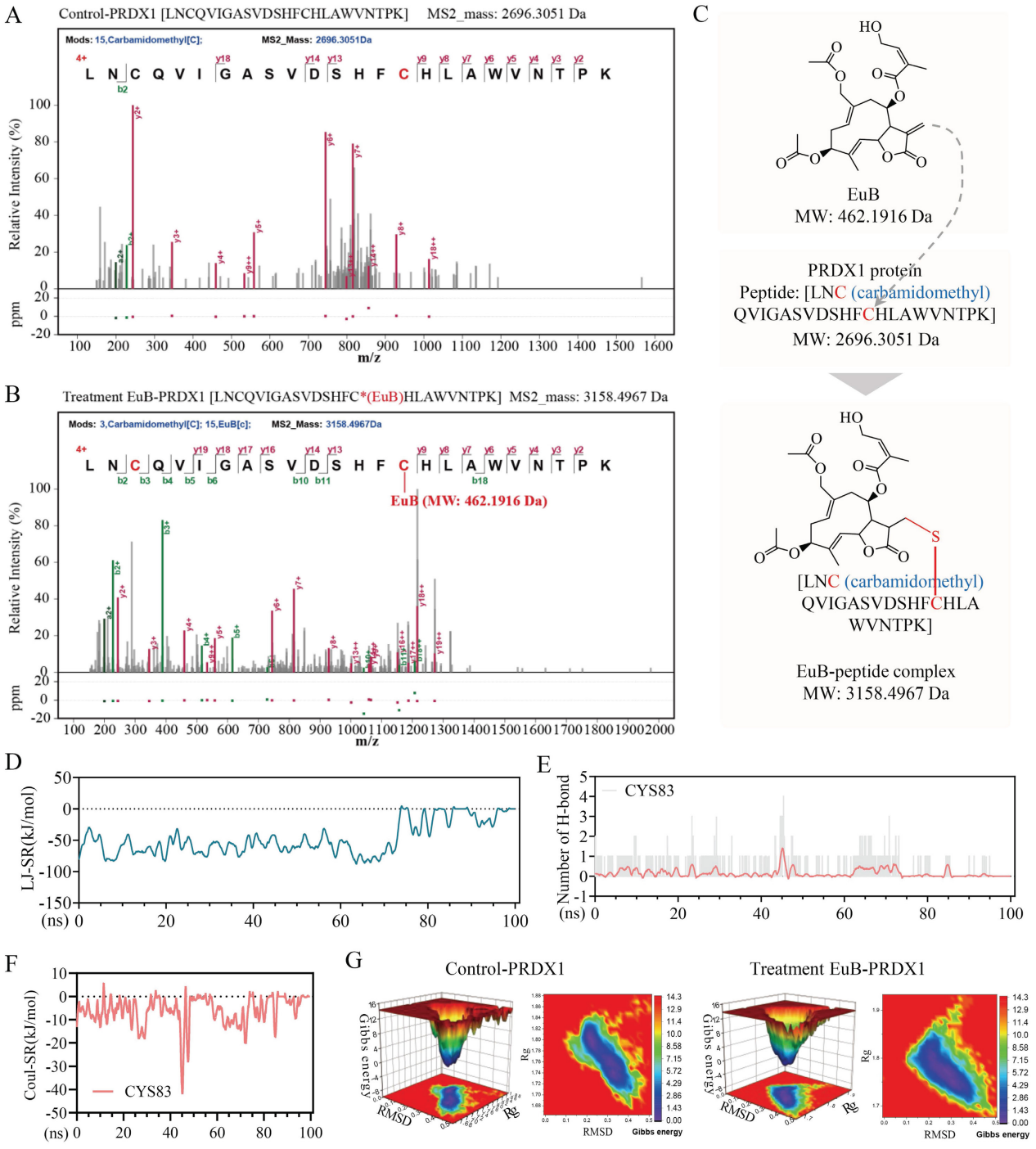


Figure 6. EuB covalently binds to the Cys83 residue of PRDX1 through its α, β-unsaturated ketone moiety. (A-B) rhPRDX1 incubated with or without EuB by MS/MS identification of peptide fragments. (C) Simulated binding model of EuB interacting with PRDX1. (D) The LJ-SR plot for EuB binding to the Cys83 residue of PRDX1. (E) The number of hydrogen bonds upon EuB binding to the Cys83 residue of PRDX1. (F) Changes in the Coul-SR for EuB binding to the Cys83 residue of PRDX1. (G) Conformational energy landscapes of PRDX1 in the absence or presence of EuB. MW, molecular weight.

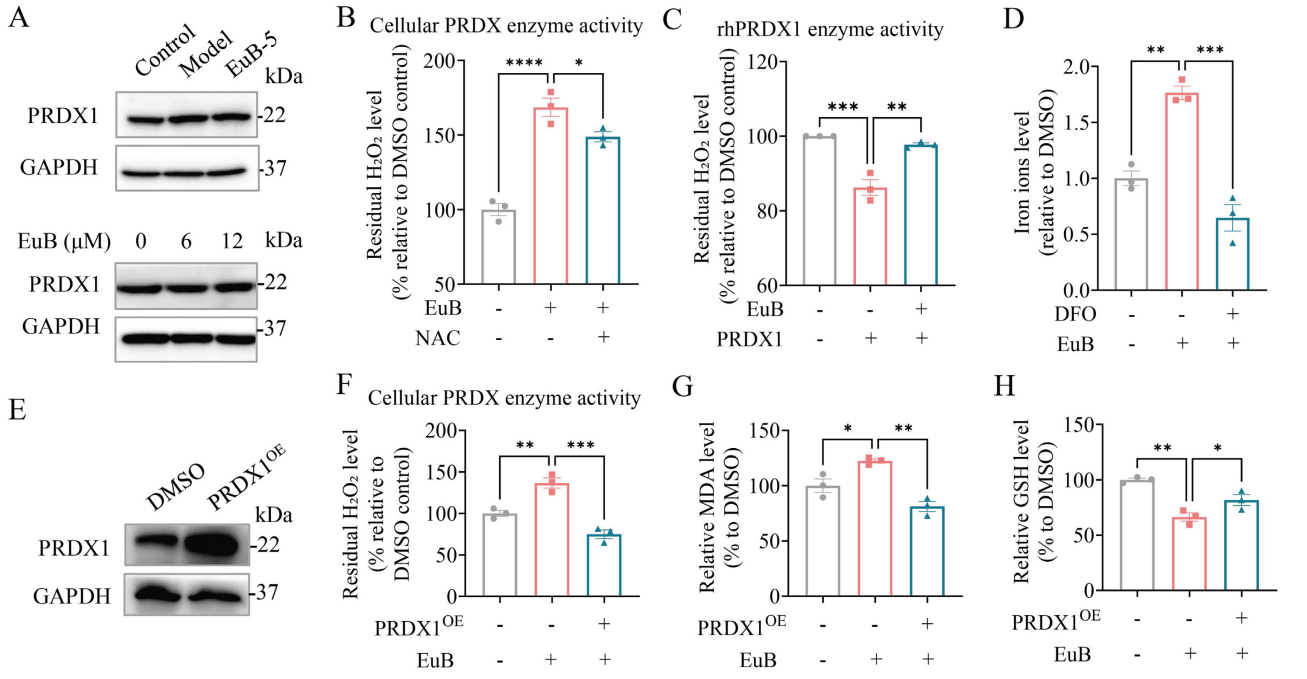


Figure 7. EuB inhibits PRDX1 enzymatic activity to induce ferroptosis in activated HSCs and exert an ameliorative effect on hepatic fibrosis. (A) Western blot of PRDX1 expression in hepatic fibrosis model and activated HSCs treated with EuB. (B) Cellular PRDX enzyme activity in activated HSCs treated with EuB (n = 3). (C) Enzymatic activity of rhPRDX1 following EuB treatment (n = 3). (D) Intracellular Fe^{2+} level in EuB-treated HSCs (n = 3). (E) Validation of PRDX1 overexpression ($PRDX1^{OE}$) in LX-2 cells by Western blot (n = 3). (F-H) Effects of $PRDX1^{OE}$ on EuB-mediated changes in cellular PRDX activity (F), MDA level (G), and GSH level (H) in activated HSCs (n = 3). Note: The PRDX peroxidase assay quantifies residual un metabolized H_2O_2; higher residual H_2O_2 signal reflects reduced PRDX peroxidase activity. Mean ± SD, *p < 0.05, **p < 0.01, ***p < 0.001, ****p < 0.0001 *vs.* PRDX1 or EuB. MDA: malondialdehyde; GSH: glutathione; GPX4: glutathione peroxidase 4.

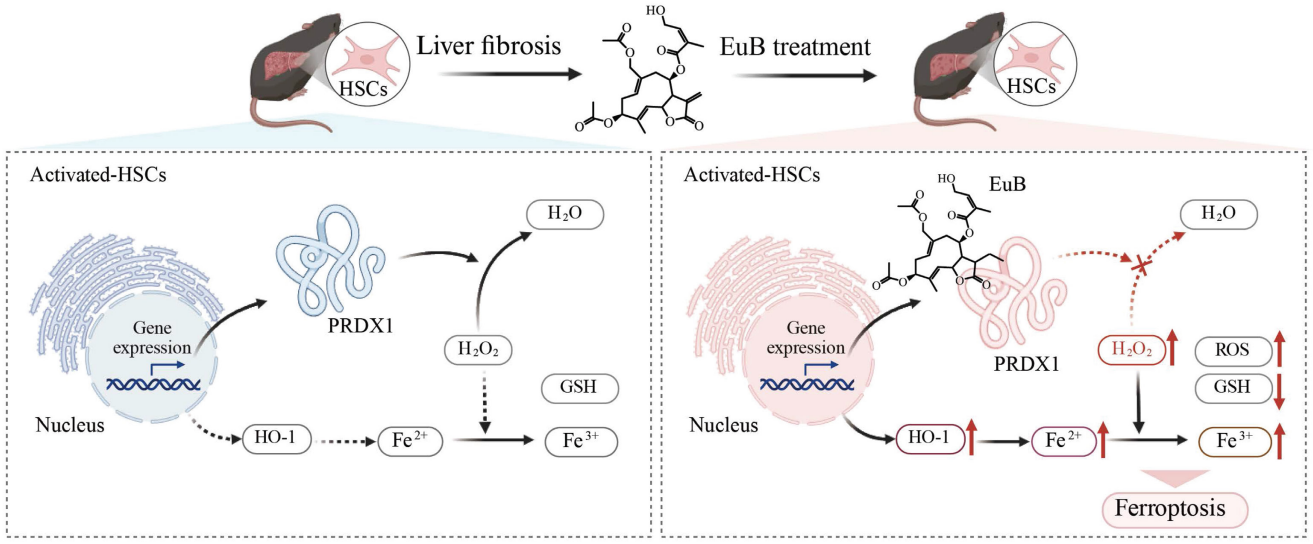


Figure 8. Schematic diagram of the mechanism in this study. EuB, a novel inhibitor of PRDX1, binds covalently to PRDX1, highlighting its great potential for the development of PRDX1-targeted anti-hepatic fibrosis agents.

Here, we first reveal that EuB, a naturally derived small molecule, effectively ameliorates hepatic fibrosis both *in vivo* and *in vitro* by activating ROS signaling pathways and inducing ferroptosis. Furthermore, we sought to deepen the understanding of the molecular mechanisms by which EuB regulates ferroptosis and ROS signaling to mediate its anti-hepatic fibrosis effects. Therefore, we synthesized an active probe (EuB-P) with alkyne-tag based on EuB to identify its direct cellular targets *via* chemical proteomics [33, 43]. Our results revealed that EuB directly binds to PRDX1 and suppresses its enzymatic activity, identifying EuB as a novel covalent inhibitor of PRDX1. Although previous studies have reported that targeting and inhibiting PRDX family proteins ameliorates hepatic fibrosis and other liver diseases [14, 44, 45], no covalent PRDXs inhibitors have been identified to date. Thus, our research fills this critical gap.

Small molecules containing an electrophilic quinone methide moiety act as Michael acceptors and covalently binds to the thiol groups of Cys residues in proteins [46, 47]. Given the presence of an α, β-unsaturated ketone moiety in EuB, we hypothesized that EuB exerts its effects by forming covalent adducts with specific Cys residues of PRDX1 through a covalent binding mechanism. Interestingly, our data showed that iodoacetamide (IAA) [48], a compound that specifically modifies protein cysteine residues, competitively reduced the binding of the EuB probe to PRDX1. Conversely, EuB could displace the IAA probe from PRDX1. Additionally, celastrol (Cel) competed with the EuB probe for PRDX1 binding. Previous studies have reported that Cel specifically binds to cysteine residues of PRDX1, including Cys53, Cys83, and Cys173, thereby impairing both the chaperone and enzymatic activities of PRDX1 [49-51]. As a classic natural product, Cel has been reported to suppress PRDX1 activity and exert anti-inflammatory, anti-cancer and anti-fibrosis effects [14, 37, 51]. However, Cel features a pentacyclic triterpenoid structure with strong non-specific binding capacity, which leads to broad-spectrum interactions with various cellular proteins and poor selectivity among PRDX family isoforms [14]. In contrast, EuB has an entirely different chemical skeleton dominated by sesquiterpene lactone. Its characteristic α, β-unsaturated ketone group acts as a key pharmacophore, enabling precise docking and binding to the specific active site of PRDX1. Moreover, EuB rarely binds to other PRDX members, such as PRDX2, which greatly reduces the risk of non-targeted responses. Given the superior structural characteristics and targeting performance, EuB holds greater potential as a selective PRDX1 inhibitor for developing targeted lead compounds. LC-MS/MS analysis confirmed that EuB forms a covalent adduct with the PRDX1-derived peptide containing the Cys83 residue. Collectively, these findings demonstrate that EuB covalently binds to PRDX1 at the Cys83 residue in a manner dependent on its α, β-unsaturated ketone moiety.

Consistent with its direct binding to the Cys residue of PRDX1, EuB effectively inhibits the PRDX1 peroxidase activity and cellular antioxidant capacity. Correspondingly, EuB induces a moderate increase in H_2O_2 levels and a decrease in GSH content in activated HSCs. Previously, it has been demonstrated that H_2O_2 abundance is closely related with ROS accumulation, lipid peroxidation, and iron metabolic homeostasis [52, 53], the dysregulation of which triggers cellular oxidative stress and ferroptosis [54]. Notably, NAC abrogated EuB-induced H_2O_2 accumulation, oxidative stress and ferroptosis in activated HSCs, strongly supporting the critical role of elevated H_2O_2 in EuB-mediated ferroptosis of activated HSCs. As a canonical suppressor of ferroptosis, GPX4 exhibits compensatory upregulation in HSCs under oxidative stress, a protective adaptive response that enables cells to resist ferroptosis [55]. However, EuB treatment reversed this compensatory GPX4 elevation, reduced the cellular threshold for ferroptosis, and ultimately facilitated the ferroptosis of activated HSCs. Mechanistically, increased H_2O_2 induces ROS generation and activates ferroptotic signaling cascades, consequently reducing GPX4 expression and GSH levels while increasing intracellular iron ion accumulation and MDA content [56-58]. These changes have been widely implicated in driving ferroptosis in activated HSCs.

One mechanism by which PRDX knockdown elevates ROS and H_2O_2 levels is the induction of ferroptosis in activated HSCs [14]. Consistent with the features of most natural products, EuB was found to bind to numerous proteins via pull-down and proteomic analysis, reflecting its broad binding spectrum [29, 59, 60]. However, gene rescue experiments clearly verified that PRDX1 overexpression could effectively restore cell function and block EuB-triggered ferroptosis. On the one hand, natural active compounds commonly bind to multiple proteins in cells, which is consistent with the characteristics of many plant-derived small molecules. On the other hand, among all potential binding partners, PRDX1 serves as the core functional target that predominantly mediates EuB's regulation of ferroptosis. Other EuB-interacting proteins may participate in auxiliary biological processes or exert weak regulatory effects, but they do not play a decisive role in this ferroptosis phenotype. This finding also further confirms the vital role of PRDX1 in the anti-fibrotic action of EuB. Collectively, EuB presents a multi-binding profile, while its anti-fibrotic effect via inducing ferroptosis is mainly dependent on targeting PRDX1.

5. Conclusions

In summary, our findings demonstrate that EuB acts as a novel selective covalent inhibitor of PRDX1, which induces ferroptosis in activated HSCs by targeting PRDX1 Cys residue, suppressing HSCs activation and collagen deposition, and ultimately ameliorating hepatic fibrosis. These results highlight EuB as a promising lead compound for the development of PRDX1-targeted therapies against hepatic fibrosis and provide a valuable chemical tool to dissect the biological functions of PRDX1 in liver disease pathogenesis.

Supplementary Material

Supplementary figures and table.
https://www.ijbs.com/v23p0391s1.pdf

Acknowledgments

The work was supported by grants from the Shenzhen Medical Research Funds (B2302051); the CACMS Innovation Fund (CI2021A05101 and CI2021A05104); the Scientific and Technological Innovation Project of China Academy of Chinese Medical Sciences (CI2021B014); Establishment of Sino-Austria "Belt and Road" Joint Laboratory on Traditional Chinese Medicine for Severe Infectious Diseases and Joint Research (2020YFE0205100); the Fundamental Research Funds for the Central Public Welfare Research Institutes (ZZ14-YQ-050, ZZ14-YQ-051, ZZ14-YQ-052, ZZ14-FL-002, ZZ14-ND-010 and ZZ15-ND-10); the Science and Technology Foundation of Shenzhen (Shenzhen Clinical Research Centre for Geriatrics); the Supported by Shenzhen key Laboratory of Kidney Diseases (SYSPG20241211173908024); the Shenzhen Fund for Guangdong Provincial High-level Clinical Key Specialties (NO.SZGSP001); Shenzhen People's Hospital Physician Scientist Training "Five Three Program" (SYWGSJCYJ202201).

Author contributions

Piao Luo, Jigang Wang, Ye Chen, Wei Xiao and Xiaoyong Zhang designed and conceived the project. Yin-Kwan Wong, Qian Zhang, Min Zou and Yu Chen conducted the animal experiments, collected the results, and wrote the original draft. Weiyi He and Yehai An performed the bioinformatics analysis. Dandan Liu, Ting Cao and Xiaoqin He carried out the cell and molecular experiments. Qiwei Zhang and Yao Liang performed the software and bioinformatics analysis and. Juyi Tian and Xuan Xiong contributed to software and formal analysis, while Piao Luo, Jigang Wang, Yin-Kwan Wong, Qian Zhang and Min Zou revised the manuscript.

Competing Interests

The authors have declared that no competing interest exists.

References

1. Borrello MT, Mann D. Chronic liver diseases: From development to novel pharmacological therapies: IUPHAR Review 37. British journal of pharmacology. 2023; 180: 2880-97.
2. Ginès P, Krag A, Abraldes JG, Solà E, Fabrellas N, Kamath PS. Liver cirrhosis. Lancet. 2021; 398: 1359-76.
3. Hammerich L, Tacke F. Hepatic inflammatory responses in liver fibrosis. Nature reviews Gastroenterology & hepatology. 2023; 20: 633-46.
4. Lieber CS. Ethanol metabolism, cirrhosis and alcoholism. Clinica chimica acta; international journal of clinical chemistry. 1997; 257: 59-84.
5. Muratori L, Lohse AW, Lenzi M. Diagnosis and management of autoimmune hepatitis. BMJ. 2023; 380: e070201.
6. Affo S, Yu LX, Schwabe RF. The Role of Cancer-Associated Fibroblasts and Fibrosis in Liver Cancer. Annual review of pathology. 2017; 12: 153-86.
7. Tsuchida T, Friedman SL. Mechanisms of hepatic stellate cell activation. Nature reviews Gastroenterology & hepatology. 2017; 14: 397-411.
8. Breitkopf-Heinlein K, Martinez-Chantar ML. Targeting hepatic stellate cells to combat liver fibrosis: where do we stand? Gut. 2024; 73: 1411-3.
9. Koda Y, Teratani T, Chu PS, Hagihara Y, Mikami Y. CD8(+) tissue-resident memory T cells promote liver fibrosis resolution by inducing apoptosis of hepatic stellate cells. Nature communications. 2021; 12: 4474.
10. Gao J, Wei B, de Assuncao TM, Liu Z, Hu X, Ibrahim S, et al. Hepatic stellate cell autophagy inhibits extracellular vesicle release to attenuate liver fibrosis. Journal of hepatology. 2020; 73: 1144-54.
11. Deng Y, Lu L, Zhu D, Zhang H, Fu Y. MafG/MYH9-LCN2 axis promotes liver fibrosis through inhibiting ferroptosis of hepatic stellate cells. Cell death and differentiation. 2024; 31: 1127-39.
12. Qu J, Li J, Wang L, Li Y, Zhang Y, Li J, et al. Disturbance of cytoskeleton induced by ligustilide promotes hepatic stellate cell senescence and ameliorates liver fibrosis. Theranostics. 2025; 15: 8049-67.
13. Lin L, Li X, Li Y, Lang Z, Li Y, Zheng J. Ginsenoside Rb1 induces hepatic stellate cell ferroptosis to alleviate liver fibrosis via the BECN1/SLC7A11 axis. Journal of pharmaceutical analysis. 2024; 14: 100902.
14. Luo P, Liu D, Zhang Q, Yang F, Wong YK, Xia F, et al. Celastrol induces ferroptosis in activated HSCs to ameliorate hepatic fibrosis via targeting peroxiredoxins and HO-1. Acta pharmaceutica Sinica B. 2022; 12: 2300-14.
15. Wood ZA, Schröder E, Robin Harris J, Poole LB. Structure, mechanism and regulation of peroxiredoxins. Trends in biochemical sciences. 2003; 28: 32-40.
16. Rhee SG, Kil IS. Multiple Functions and Regulation of Mammalian Peroxiredoxins. Annual review of biochemistry. 2017; 86: 749-75.
17. Stöcker S, Maurer M, Ruppert T, Dick TP. A role for 2-Cys peroxiredoxins in facilitating cytosolic protein thiol oxidation. Nature chemical biology. 2018; 14: 148-55.
18. Bolduc J, Koruza K, Luo T, Malo Pueyo J, Vo TN, Ezeriņa D, et al. Peroxiredoxins wear many hats: Factors that fashion their peroxide sensing personalities. Redox biology. 2021; 42: 101959.
19. Chen C, Gong L, Liu X, Zhu T, Zhou W, Kong L, et al. Identification of peroxiredoxin 6 as a direct target of withangulatin A by quantitative chemical proteomics in non-small cell lung cancer. Redox biology. 2021; 46: 102130.
20. Winterbourn CC. Peroxiredoxins: Antioxidant Activity, Redox Relays, and Redox Signaling. Biochemistry. 2025; 64: 4477-86.
21. Ledgerwood EC, Marshall JW, Weijman JF. The role of peroxiredoxin 1 in redox sensing and transducing. Archives of biochemistry and biophysics. 2017; 617: 60-7.
22. Yin W, Xu H, Bai Z, Wu Y, Zhang Y, Liu R, et al. Inhibited peroxidase activity of peroxiredoxin 1 by palmitic acid exacerbates nonalcoholic steatohepatitis in male mice. Nature communications. 2025; 16: 598.
23. Yuan J, Yu Z, Zhang P, Luo K, Xu Y, Lan T, et al. DDAH1 recruits peroxiredoxin 1 and sulfiredoxin 1 to preserve its activity and regulate intracellular redox homeostasis. Redox biology. 2024; 70: 103080.
24. Jia K, Ma Z, Zhang Y, Xie K, Li J, Wu J, et al. Picroside II promotes HSC apoptosis and inhibits the cholestatic liver fibrosis in Mdr2(-/-) mice by polarizing M1 macrophages and balancing immune responses. Chinese journal of natural medicines. 2024; 22: 582-98.
25. Wei M, Zhang Y, Sun X, Qi L, Liu Q. The potential therapeutic role of ginsenosides on fibrosis-associated diseases: a review on molecular mechanisms and call for further research. Chinese journal of natural medicines. 2025; 23: 673-86.
26. Chen S, Li R, Zhang C, Guo J, Yang A, Yang D, et al. Baicalein Induces Hepatic Stellate Cell Senescence and Attenuates Liver Fibrosis via CEBPZ/p53/HK2-Mediated Glycolysis Inhibition. Phytomedicine. 2025; 148: 157222.
27. Han X, Ning Y, Dou X, Wang Y, Shan Q, Shi K, et al. Cornus officinalis with high pressure wine steaming enhanced anti-hepatic fibrosis: Possible through SIRT3-AMPK axis. Journal of pharmaceutical analysis. 2024; 14: 100927.
28. Zhang Q, Luo P, Zheng L, Chen J, Zhang J, Tang H, et al. 18beta-glycyrrhetinic acid induces ROS-mediated apoptosis to ameliorate hepatic fibrosis by targeting PRDX1/2 in activated HSCs. Journal of pharmaceutical analysis. 2022; 12: 570-82.
29. Kuang W, Zhuge R, Song P, Yi L, Zhang S, Zhang Y, et al. Eupalinolide B inhibits periodontitis development by targeting ubiquitin conjugating enzyme UBE2D3. MedComm. 2025; 6: e70034.
30. Huang L, Li G, Zhang Y, Zhuge R, Qin S, Qian J, et al. Small-molecule targeting BCAT1-mediated BCAA metabolism inhibits the activation of SHOC2-RAS-ERK to induce apoptosis of Triple-negative breast cancer cells. Journal of advanced research. 2025; 75: 723-38.
31. Wang B, Li H, Gill G, Zhang X, Tao G, Liu B, et al. Hepatic Surf4 Deficiency Impairs Serum Amyloid A1 Secretion and Attenuates Liver Fibrosis in Mice. Research. 2024; 7: 1-14.
32. Jia H, Li J, Chen X, Liu Z, Wu C, Liu C, et al. ErTao decoction alleviates liver fibrosis by suppressing STING-mediated macrophages and NLRP3 inflammasome activation. Phytomedicine. 2025; 139: 156489.
33. Luo P, Zhang Q, Shen S, An Y, Yuan L, Wong YK, et al. Mechanistic engineering of celastrol liposomes induces ferroptosis and apoptosis by directly targeting VDAC2 in hepatocellular carcinoma. Asian journal of pharmaceutical sciences. 2023; 18: 100874.

34. He H, Hao M, Luo P, Chen J, An Y, Huang J, et al. Inhibition Peroxiredoxin-2 by Capsaicin Ameliorates Rheumatoid Arthritis via ROS-Mediated Apoptosis in Fibroblast-Like Synoviocytes. MedComm. 2025; 6: e70209.
35. Luo P, Chen J, An Y, Meng K, Zhou W, Li W, et al. Icaritin Ameliorates Cisplatin-Induced Mitochondrial Metabolic Dysfunction-Associated Nephrotoxicity and Synergistically Potentiates Its Antitumor Efficacy. Advanced science. 2026; 13: e06712.
36. Gao P, Wang J, Qiu C, Zhang H, Wang C, Zhang Y, et al. Photoaffinity probe-based antimalarial target identification of artemisinin in the intraerythrocytic developmental cycle of Plasmodium falciparum. iMeta. 2024; 3: e176.
37. Chen X, Zhao Y, Luo W, Chen S, Lin F, Zhang X, et al. Celastrol induces ROS-mediated apoptosis via directly targeting peroxiredoxin-2 in gastric cancer cells. Theranostics. 2020; 10: 10290-308.
38. Gozzelino R, Jeney V, Soares MP. Mechanisms of cell protection by heme oxygenase-1. Annual review of pharmacology and toxicology. 2010; 50: 323-54.
39. Aeby E, Ahmed W, Redon S, Simanis V, Lingner J. Peroxiredoxin 1 Protects Telomeres from Oxidative Damage and Preserves Telomeric DNA for Extension by Telomerase. Cell reports. 2016; 17: 3107-14.
40. Jeong SJ, Kim S, Park JG, Jung IH, Lee MN, Jeon S, et al. Prdx1 (peroxiredoxin 1) deficiency reduces cholesterol efflux via impaired macrophage lipophagic flux. Autophagy. 2018; 14: 120-33.
41. Zhu YY, Chen S, Zhang SN, Zhu YS, Liang JY, Wang ZY, et al. Design and evaluation of peroxiredoxin 1 agonist based on scaffold hopping of salvianolic acids and combinatorial click chemistry. Acta pharmacologica sinica. 2026; 47: 1965-79.
42. He Y, Li S, Tang D, Peng Y, Meng J, Peng S, et al. Circulating Peroxiredoxin-1 is a novel damage-associated molecular pattern and aggravates acute liver injury via promoting inflammation. Free radical biology & medicine. 2019; 137: 24-36.
43. An Y, Zhang Q, Chen Y, Xia F, Wong YK, He H, et al. Chemoproteomics Reveals Glaucocalyxin A Induces Mitochondria-Dependent Apoptosis of Leukemia Cells via Covalently Binding to VDAC1. Advanced biology. 2024; 8: e2300538.
44. Park J, Kim NH, Yi HJ, Rhee SG, Woo HA. Mitochondrial Peroxiredoxin III Protects against Non-Alcoholic Fatty Liver Disease Caused by a Methionine-Choline Deficient Diet. Antioxidants. 2022; 12.
45. Kim MH, Seong JB, Huh JW, Bae YC, Lee HS, Lee DS. Peroxiredoxin 5 ameliorates obesity-induced non-alcoholic fatty liver disease through the regulation of oxidative stress and AMP-activated protein kinase signaling. Redox biology. 2020; 28: 101315.
46. Zhang D, Chen Z, Hu C, Yan S, Li Z, Lian B, et al. Celastrol binds to its target protein via specific noncovalent interactions and reversible covalent bonds. Chemical communications. 2018; 54: 12871-4.
47. Liu CX, Yin QQ, Zhou HC, Wu YL, Pu JX, Xia L, et al. Adenanthin targets peroxiredoxin I and II to induce differentiation of leukemic cells. Nature chemical biology. 2012; 8: 486-93.
48. Abo M, Li C, Weerapana E. Isotopically-Labeled Iodoacetamide-Alkyne Probes for Quantitative Cysteine-Reactivity Profiling. Molecular pharmaceutics. 2018; 15: 743-9.
49. Chen S, Wang Z, Gao J, Wang Y, Liang J, Zhu Y, et al. Rapid Discovery of Celastrol Derivatives as Potent and Selective PRDX1 Inhibitors via Microplate-Based Parallel Compound Library and *In Situ* Screening. Journal of medicinal chemistry. 2025; 68: 13609-27.
50. Zhao Q, Ding Y, Deng Z, Lee OY, Gao P, Chen P, et al. Natural products triptolide, celastrol, and withaferin A inhibit the chaperone activity of peroxiredoxin I. Chemical science. 2015; 6: 4124-30.
51. Xu H, Zhao H, Ding C, Jiang D, Zhao Z, Li Y, et al. Celastrol suppresses colorectal cancer via covalent targeting peroxiredoxin 1. Signal transduction and targeted therapy. 2023; 8: 51.
52. Xu B, Deng Y, Dai W, Shang Y, Ding L, Zhang Z, et al. 3D cultured human umbilical cord mesenchymal stem cell spheroids regulate oxidative stress and iron homeostasis through the Nrf2 pathway to resist ferroptosis in ovarian granulosa cells and ovarian dysfunction. Free radical biology & medicine. 2025; 236: 28-40.
53. Li Y, Han S, Zhao Y, Yan J, Luo K, Li F, et al. A Redox-Triggered Polymeric Nanoparticle for Disrupting Redox Homeostasis and Enhanced Ferroptosis. Small. 2025; 21: e2404299.
54. Dixon SJ. Epigenetic Regulation of Ferroptosis in the Liver. Research. 2024; 7: 0323.
55. Huang B, Wang H, Liu S, Hao M, Luo D, Zhou Y, et al. Palmitoylation-dependent regulation of GPX4 suppresses ferroptosis. Nature communications. 2025; 16: 867.
56. Chen Y, Guo X, Zeng Y, Mo X, Hong S, He H, et al. Oxidative stress induces mitochondrial iron overload and ferroptotic cell death. Scientific reports. 2023; 13: 15515.
57. Su LJ, Zhang JH, Gomez H, Murugan R, Hong X, Xu D, et al. Reactive Oxygen Species-Induced Lipid Peroxidation in Apoptosis, Autophagy, and Ferroptosis. Oxidative medicine and cellular longevity. 2019; 2019: 5080843.
58. He R, Wei Y, Peng Z, Yang J, Zhou Z, Li A, et al. α-Ketoglutarate alleviates osteoarthritis by inhibiting ferroptosis via the ETV4/SLC7A11/GPX4 signaling pathway. Cellular & molecular biology letters. 2024; 29: 88.
59. Li H, Li G, Huang L, Fan T, Zhang Y, Zhang J, et al. Eupalinolide B Ameliorates Diabetic Kidney Disease via Inhibition of Cell Division Cycle 37-Mediated Inflammatory Pathways. Journal of the american society of nephrology. 2026; 37: 2146-61.
60. Luo W, Zhuang Y, Shen S, Wang Y, Zhu Y, Liu Y, et al. Eupalinolide B alleviates ulcerative colitis by targeting HMGB1 through modulation of the HMGB1/TLR4/MyD88/NF-κB signaling pathway. Phytomedicine. 2026; 156: 158245.